ELSEVIER

Journal of Computational and Applied Mathematics 101 (1999) 131–152

JOURNAL OF COMPUTATIONAL AND APPLIED MATHEMATICS

A fed back level-set method for moving material–void interfaces[1]

B. Koren[a,*], A.C.J. Venis[b]

[a] *CWI, P.O. Box 94079, 1090 GB Amsterdam, The Netherlands*

[b] *MacNeal-Schwendler (E.D.C.) B.V. Groningenweg 6, 2803 PV Gouda, The Netherlands*

Abstract

This report is a feasibility study of a level-set method for the computation of moving material–void interfaces in an Eulerian formulation. The report briefly introduces level-set methods and focuses on the development of such a method, that does not just accurately resolve the geometry of the interface, but also the physical quantities at and near the interface. Results are presented for illustrative model problems. As concerns its ability to improve the geometrical resolution of free boundaries, as expected, the level-set method performs excellently. Concerning the improvement of physical (all other than merely geometrical) free-boundary properties, the method performs very well for downstream-facing fronts and is promising for upstream-facing ones. © 1999 Elsevier Science B.V. All rights reserved.

AMS classification: 65M20; 65M99; 76M99; 76T05

Keywords: Free-boundary problems; Material–void interfaces; Discretization of convection equations; Level-set methods

1. Introduction

1.1. Problem definition

The subject of this paper is the investigation and further development of a numerical method which is promising for the computation of a special class of free-boundary problems: moving material interfaces, in application areas such as forging and sloshing. Particularly in the first application area, the accuracy requirements imposed on the geometrical and physical resolution of the interface are very high. (With physical resolution we mean that of quantities such as velocity, density, stresses, etc.) In both applications, in general, proper use may be made of the property that at one side of the

* Corresponding author. Tel.: +31.205924114; fax: +31. 205924199; e-mail: barry.koren@cwi.nl.

[1] This research was performed for MacNeal-Schwendler (E.D.C.) B.V., and was financially supported by the Netherlands Ministry of Economic Affairs, through its programme *Senter*.

0377-0427/99/$ – see front matter © 1999 Elsevier Science B.V. All rights reserved.
PII: S0377-0427(98)00203-9

interface, the material can be modeled as void. E.g., with steel and air at either side of the interface, the modeling of air as void is quite realistic. In the present paper, material–void interfaces will be considered only. For reasons of transparency, the numerical methods considered are not applied to real interface problems, but to clarifying model problems with known exact solutions.

1.2. Existing computational approaches

The existing computational approaches for free-boundary problems are Lagrangian, Eulerian or a combination of both: Arbitrary Lagrangian–Eulerian (ALE). In the Lagrangian approach, the grid is attached to the free boundary. As a consequence, the fronts resolved in this way are crisp. But they are not necessarily accurate; their location, even their topology, may be inaccurate. A known drawback of the Lagrangian approach is that it is not well-suited for the computation of bifurcating free boundaries. The Eulerian approach, in which the front moves through a grid which is fixed in space, does not have this drawback, but — as is known — here the fronts are diffused. The ALE technique attempts to avoid both drawbacks. In it, a grid is attached to the front, but it is remeshed in due time, after great distortions or bifurcations. In case of rapid great distortions or rapid bifurcations, frequent remeshing is needed, which is disadvantageous of course. In the present paper, we consider the pure Eulerian approach only.

In the pure Eulerian approach, since many years, some well-proven techniques exist for computing free-boundary flows. Known examples of these are the marker-and-cell (MAC) method (see, e.g., [7]) and the volume-of-fluid (VOF) method (see, e.g., [4, 8]). Both methods have as a drawback that they may require intricate (subcell) bookkeeping to properly keep track of fronts. (In case of MAC, the subcell bookkeeping consists of investigating whether possibly occurring cavitating cells are either numerical or physical.) In principle, all this bookkeeping can be avoided in a more recent class of computing methods for free-boundary flows: the so-called level-set methods. A text book on level-set methods is [17], a classical journal paper is [15]. Since [15], many more journal papers have appeared on level-set methods, various of these directed towards fluid-flow applications (see, e.g., [2, 3, 5, 6, 9, 13, 18, 20]). In all these papers, the interfaces considered are of material–material type. Material–void interfaces, the subject of this paper, seem to be novel.

1.3. Level-set methods

Because of their nonsmoothness, moving fronts cannot be captured sufficiently accurate on fixed grids. No advantage can be taken of nice numerical accuracy properties, valid for smooth solutions only. As a natural fix to this, in the level-set method, to the system of physical unknowns, a nonphysical unknown is added, which *is* smooth at the front: the level-set function. Furthermore, a nonphysical equation is added: a convection equation for the level-set function. E.g, to the Euler equations written in conservative variables, one may add the level-set function $\psi=\psi(x,y,z,t)$, which is convected as — in principle — a passive scalar, by the likewise conservative equation

$$\frac{\partial(\rho\psi)}{\partial t}+\frac{\partial(\rho u\psi)}{\partial x}+\frac{\partial(\rho v\psi)}{\partial y}+\frac{\partial(\rho w\psi)}{\partial z}=0. \tag{1.1}$$

This leads to the extended system

$$\frac{\partial q}{\partial t}+\frac{\partial f(q)}{\partial x}+\frac{\partial g(q)}{\partial y}+\frac{\partial h(q)}{\partial z}=0, \tag{1.2a}$$

$$q=\begin{pmatrix}\rho\\ \rho u\\ \rho v\\ \rho w\\ \rho e\\ \rho\psi\end{pmatrix}, \tag{1.2b}$$

$$f(q)=\begin{pmatrix}\rho u\\ \rho u^2+p\\ \rho uv\\ \rho uw\\ \rho u(e+\frac{p}{\rho})\\ \rho u\psi\end{pmatrix},\quad g(q)=\begin{pmatrix}\rho v\\ \rho vu\\ \rho v^2+p\\ \rho vw\\ \rho v(e+\frac{p}{\rho})\\ \rho v\psi\end{pmatrix},\quad h(q)=\begin{pmatrix}\rho w\\ \rho wu\\ \rho wv\\ \rho w^2+p\\ \rho w(e+\frac{p}{\rho})\\ \rho w\psi\end{pmatrix}. \tag{1.2c}$$

Note that in system (1.2), ψ is a passive scalar indeed; there is no feedback of the convection of ψ into that of mass, momentum or energy. If one is only interested in an accurate geometrical resolution of the interface, in principle, a feedback is not necessary. In case of a free-boundary computation of, e.g., two nonmixing gases at different densities, the standard Eulerian difficulty to accurately resolve the geometry of the discontinuous gas interface may be directly alleviated by taking for the level-set function an initial solution which is smooth everywhere (so also at the initial gas interface) and which has a pre-defined and constant value at the interface, a value which exists at the interface only. Then it is clear that to accurately resolve the gas interface — instead of following the density jump – one can better keep track of this pre-defined interface value for ψ — say ψ_f — because one can take maximal advantage of the smoothness of ψ. (For the density, the accuracy properties of most higher-order accurate discretizations break down at precisely the point of interest: the interface.) This easy possibility for creating smoothness at the interface (through a smooth, artificial, passive scalar function) is a first interesting property of the level-set method. Related to this, a second interesting property is that the interface location is neatly defined (viz., as the location where $\psi=\psi_f$). With a physical jump at the interface from, say, $c=1$ to $c=0$ (where c models, e.g., the material density), in case of a diffused grid-representation of this jump, it is not immediately clear how to precisely define the interface location. (Should one define it as there where $c=\frac{1}{2}$ or $c=h$, with h the mesh size, or as whatever?) A third interesting property of the level-set technique is that the level-set function ψ requires no new, specifically tailored discretization method. The discretization method that one has in mind for the physical system, can be easily and consistently extended with the new conservation equation for $\rho\psi$. So, as opposed to fluid markers or volume-of-fluid fractions, the level-set function can be directly and consistently embedded in the existing, discrete system of physical equations. Related to this, a fourth advantage of level-set methods is that there is no difficulty in extending the system of equations from 2-D to 3-D.

When one is not only interested in an accurate geometrical resolution of the interface, but also in an improved resolution of physical quantities at and near the interface, the level-set approach still

offers a possibility that seems to be new. A physically sound feedback of the level-set function may be incorporated into the real (physical) equations. In all level-set literature known to us, if there is a feedback of the level-set function ψ into physics, it is restricted to material properties such as the ratio of specific heats ($\gamma = \gamma(\psi)$) and the kinematic viscosity ($\nu = \nu(\psi)$). In the present paper, the level-set function will be explicitly fed back into the computation of the physical flux function $f = f(c)$. I.e., in the discrete case, we extend this to $f = f(c, \psi)$.

The contents of the paper is the following. In Section 2, we present two model problems to be considered throughout this paper and we present reference results for it. In Section 3, a standard level-set method is considered, one without feedback into the physical system. Simple shape-tracking results are presented for it. The level-set method with feedback is presented in Section 4, together with results for the two test cases. Concluding remarks are given in Section 5.

2. Test cases and reference results

2.1. Model problems and exact discrete solutions

In the model problems to be considered, the multi-dimensional convection of an interface is the issue. In here, as mentioned, we are not only interested in shape preservation. The problems are described by the 2-D, linear, unsteady convection equation

$$\frac{\partial c}{\partial t} + u\frac{\partial c}{\partial x} + v\frac{\partial c}{\partial y} = 0, \quad (x, y) \in [-1, 1] \times [-1, 1], \tag{2.1}$$

with as initial conditions:

$$c(x, y, t = 0) = \begin{cases} 1, & (x, y) \in (x - x_c)^2 + (y - y_c)^2 \leqslant (\frac{1}{5})^2, \quad x_c = y_c = -\frac{1}{2}, \\ 0 & \text{elsewhere,} \end{cases} \tag{2.2a}$$

and

$$c(x, y, t = 0) = \begin{cases} 1, & (x, y) \in [x_c - \frac{1}{5}, y_c - \frac{1}{5}] \times [x_c + \frac{1}{5}, y_c + \frac{1}{5}], \quad x_c = y_c = -\frac{1}{2}; \\ 0 & \text{elsewhere.} \end{cases} \tag{2.2b}$$

For the velocity field, defined for positive c only (i.e., in the material only), we simply take

$$u = v = 1, \tag{2.3}$$

and for the inlet boundary conditions we take

$$c(x = -1, y, t) = c(x, y = -1, t) = 0. \tag{2.4}$$

So, the problems describe the diagonal transport in a square domain, of successively a circular initial solution, (2.2a), and a square initial solution, (2.2b). Requested for both the circle and the square: $c(x, y, t = 1)$. The exact solutions are identical to the initial solutions (2.2a) and (2.2b), but now with $x_c = y_c = \frac{1}{2}$. (For other initial values of x_c and y_c, this problem was already considered in [1].)

Both problems are solved on equidistant, cell-centered finite-volume grids with successively 20×20, 40×40 and 80×80 cells, so for $h_x = h_y = h = \frac{1}{10}, \frac{1}{20}$ and $\frac{1}{40}$. Fig. 1 shows iso-line distributions of the initial solutions and the final, exact discrete solutions. (The iso-lines are given at $c = 0.1n, n = 1, \ldots, 9$.)

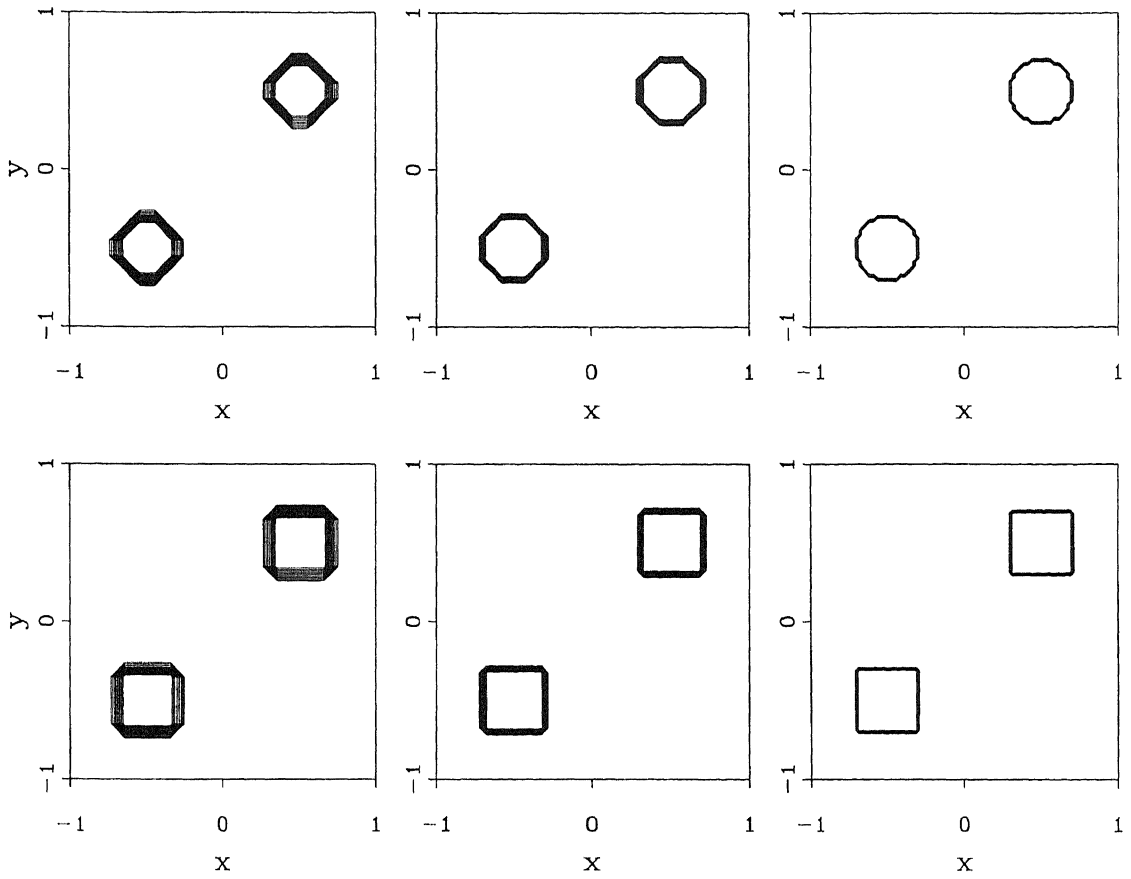

Fig. 1. Intial and final exact discrete solutions for convection circle (up) and square (down), for from left to right: $h = \frac{1}{10}, \frac{1}{20}, \frac{1}{40}$.

2.2. Standard numerical method

The cell-centered finite-volume discretization of the integral form of (2.1) yields, on an equidistant grid with $h_x = h_y = h$, the semi-discrete equation

$$\frac{1}{h}\int\int \frac{\partial c}{\partial t}\,\mathrm{d}x\,\mathrm{d}y + u(c_{i+1/2,j} - c_{i-1/2,j}) + v(c_{i,j+1/2} - c_{i,j-1/2}) = 0. \tag{2.5}$$

In here, the half-integer indices $i - \frac{1}{2}, j$ and $i + \frac{1}{2}, j$ refer to the vertical cell faces $\partial\Omega_{i-1/2,j}$ and $\partial\Omega_{i+1/2,j}$, in between the cells $\Omega_{i-1,j}$ and $\Omega_{i,j}$, and $\Omega_{i,j}$ and $\Omega_{i+1,j}$, respectively (Figure 2). Likewise, the indices $i, j - \frac{1}{2}$ and $i, j + \frac{1}{2}$ refer to the horizontal cell faces $\partial\Omega_{i,j-1/2}$ and $\partial\Omega_{i,j+1/2}$, separating $\Omega_{i,j-1}$ and $\Omega_{i,j}$, and $\Omega_{i,j}$ and $\Omega_{i,j+1}$ (Fig. 2).

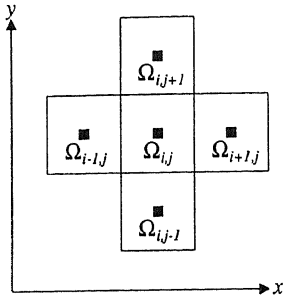

Fig. 2. Cell-centered finite volume $\Omega_{i,j}$ with nearest neighbors.

We proceed by giving the standard numerical scheme for computing the cell-face fluxes in the present two problems. At the vertical cell faces $\partial\Omega_{i+1/2,j}$, $i=0,1,\ldots,n$, $j=1,2,\ldots,n$ we apply

$$c_{i+\frac{1}{2},j}=\begin{cases} i=0: & (c_{\text{exact}})_{1/2,j}=0,\\ i=1: & \frac{1}{2}(c_{1,j}+c_{2,j}),\\ i=n: & c_{n,j}+\frac{1}{2}(c_{n,j}-c_{n-1,j}),\\ \text{else:} & c_{i,j}+\frac{1}{2}\phi(r_{i+1/2,j})(c_{i,j}-c_{i-1,j}), \quad r_{i+1/2,j}\equiv\frac{c_{i+1,j}-c_{i,j}+\varepsilon}{c_{i,j}-c_{i-1,j}+\varepsilon},\ 0<\varepsilon\ll 1, \end{cases} \tag{2.6a}$$

and likewise, at the horizontal cell faces $\partial\Omega_{i,j+1/2}$, $i=1,2,\ldots,n$, $j=0,1,\ldots,n$

$$c_{i,j+\frac{1}{2}}=\begin{cases} j=0: & (c_{\text{exact}})_{i,1/2}=0,\\ j=1: & \frac{1}{2}(c_{i,1}+c_{i,2}),\\ j=n: & c_{i,n}+\frac{1}{2}(c_{i,n}-c_{i,n-1}),\\ \text{else:} & c_{i,j}+\frac{1}{2}\phi(r_{i,j+1/2})(c_{i,j}-c_{i,j-1}), \quad r_{i,j+1/2}\equiv\frac{c_{i,j+1}-c_{i,j}+\varepsilon}{c_{i,j}-c_{i,j-1}+\varepsilon},\ 0<\varepsilon\ll 1. \end{cases} \tag{2.6b}$$

As the limiter $\phi=\phi(r)$, we apply

$$\phi(r)=\begin{cases} 0, & r<0,\\ 2r, & 0<r\leqslant\frac{2}{5},\\ \frac{4}{5}, & \frac{2}{5}<r\leqslant\frac{7}{10},\\ \frac{1}{3}+\frac{2}{3}r, & \frac{7}{10}<r\leqslant\frac{5}{2},\\ 2 & \text{else.} \end{cases} \tag{2.7}$$

This limiter is a more accurate version of the $\kappa=\frac{1}{3}$-limiter presented in [11]. Concerning its TVD-properties, it can be directly seen that limiter (2.7) fits into Sweby's TVD domain [19]:

$$0\leqslant\phi(r)\leqslant\min(2r,2) \quad \text{for } r\geqslant 0, \tag{2.8a}$$

$$\phi(r)=0 \quad \text{for } r\leqslant 0. \tag{2.8b}$$

Concerning the accuracy properties of (2.7), while the $\kappa=\frac{1}{3}$-limiter from [11] is formally third-order accurate in monotonous, smooth flow parts only (most limiters are second-order accurate there), the

new $\kappa = \frac{1}{3}$-limiter (2.7) also gives third-order accuracy in smooth extrema. To show these good accuracy properties, consider the 1-D model equation $dc/dx = 0$. The corresponding equation for finite volume Ω_i reads

$$c_{i+1/2} - c_{i-1/2} = 0, \tag{2.9}$$

where $c_{i+1/2}$ and $c_{i-1/2}$ are the two cell-face fluxes, for which we take

$$c_{i+1/2} = c_i + \frac{1}{2}\phi(r_{i+1/2})(c_i - c_{i-1}), \quad r_{i+1/2} = \frac{c_{i+1} - c_i}{c_i - c_{i-1}}, \tag{2.10a}$$

$$c_{i-1/2} = c_i + \frac{1}{2}\phi(r_{i-1/2})(c_{i-1} - c_{i-2}), \quad r_{i-1/2} = \frac{c_i - c_{i-1}}{c_{i-1} - c_{i-2}}. \tag{2.10b}$$

(The ε present in (2.6) has been omitted here; it is meant to avoid division by zero in practice, in the situation of a locally constant flow field.) Let us first consider the situation of a locally, monotonously increasing or decreasing solution and next that of a smooth extremum.

Locally monotonous solution. For this situation, through Taylor-series expansion around c_i, for $r_{i+1/2}$ and $r_{i-1/2}$ we find

$$r_{i+1/2} = 1 + h\,\frac{d^2c_i}{dx^2} \Big/ \frac{dc_i}{dx} + \mathcal{O}(h^2), \tag{2.11a}$$

$$r_{i-1/2} = 1 + h\,\frac{d^2c_i}{dx^2} \Big/ \frac{dc_i}{dx} + \mathcal{O}(h^2). \tag{2.11b}$$

Hence, both $\phi(r_{i+1/2})$ and $\phi(r_{i-1/2})$ in (2.10a) and (2.10b), respectively, have to be expanded around $r = 1$. Doing so, after further expansion around c_i, from (2.9) and (2.10) it follows the modified equation

$$\frac{dc}{dx} - \frac{1}{2}h(1 - \phi(1))\frac{d^2c}{dx^2} + \frac{1}{6}h^2\left(1 - 3\phi(1) + 3\frac{d\phi(1)}{dr}\right)\frac{d^3c}{dx^3} = \mathcal{O}(h^3). \tag{2.12}$$

So, to get third-order accuracy in monotonous flow regions, the limiter function $\phi(r)$ must satisfy

$$\phi(1) = 1, \tag{2.13a}$$

$$\frac{d\phi(1)}{dr} = \frac{2}{3}. \tag{2.13b}$$

Limiter (2.7) satisfies these requirements (as does the old limiter from [11]).

Smooth extremum. For a smooth extremum, through Taylor-series expansion around c_i, and through the assumption that the extremum coincides with the cell center i (i.e., $dc_i/dx = 0$), we find

$$r_{i+1/2} = -1 - \frac{2}{3}h\,\frac{d^3c_i}{dx^3} \Big/ \frac{d^2c_i}{dx^2} + \mathcal{O}(h^2), \tag{2.14a}$$

$$r_{i-1/2} = \frac{1}{3} + \frac{4}{27}h \frac{\mathrm{d}^3 c_i}{\mathrm{d}x^3} \Big/ \frac{\mathrm{d}^2 c_i}{\mathrm{d}x^2} + \mathcal{O}(h^2). \tag{2.14b}$$

Expanding next $\phi(r_{i+1/2})$ around -1, $\phi(r_{i-1/2})$ around $\frac{1}{3}$ and next all terms around c_i, from (2.9) and (2.10) we now get the modified equation

$$\frac{1}{4}h\left(-\phi(-1) - 2 + 3\phi\left(\frac{1}{3}\right)\right)\frac{\mathrm{d}^2 c}{\mathrm{d}x^2} + \frac{1}{3}h^2\left(\frac{1}{4}\phi(-1) + \frac{1}{2}\frac{\mathrm{d}\phi(-1)}{\mathrm{d}r} + \frac{1}{2} - \frac{7}{4}\phi\left(\frac{1}{3}\right) + \frac{1}{3}\frac{\mathrm{d}\phi(\frac{1}{3})}{\mathrm{d}r}\right)\frac{\mathrm{d}^3 c}{\mathrm{d}x^3} = \mathcal{O}(h^3). \tag{2.15}$$

Sticking to Sweby's TVD domain, i.e., to $\phi(-1) = 0$ and $\mathrm{d}\phi(-1)/\mathrm{d}r = 0$, from (2.15) it follows as accuracy requirements

$$\phi(\tfrac{1}{3}) = \tfrac{2}{3}, \tag{2.16a}$$

$$\frac{\mathrm{d}\phi(\frac{1}{3})}{\mathrm{d}r} = 2. \tag{2.16b}$$

Limiter (2.7) satisfies these additional requirements. (The limiter from [11] does not.) The standard space discretization has been defined now.

Time integration. For the time integration we simply take the standard, four-stage Runge–Kutta scheme, which is fourth-order time-accurate for nonlinear problems. In all computational results to be presented hereafter, the time step is taken linearly proportional to the mesh size, and sufficiently small to ensure that time discretization errors are negligible with respect to space discretization errors. I.e., in all cases we take $\sqrt{u^2 + v^2}\Delta t/h \leqslant \frac{1}{2}$. According to [10], stability and monotonicity are guaranteed by these small time steps.

Reference results. In Fig. 3, as in Fig. 1, we give the iso-line distributions of the initial and final solutions. (Iso-lines are given again at $c = 0.1n, n = 1,\ldots,9$.) In Table 1, some more quantitative information is given about these numerical solutions. In here, $\|\Delta c\|_1$ and $\|\Delta c\|_\infty$ are the L_1- and L_∞-norms of the solution errors. Due to the being discontinuous of both initial solutions, we observe a first-order accuracy behavior in $\|\Delta c\|_1$ and a zeroth-order behavior in $\|\Delta c\|_\infty$.

3. Present level-set method

3.1. Principle

To explain the principle of the present level-set method — first without feedback — for transparency reasons we consider the 1-D convection equation

$$\frac{\partial c}{\partial t} + u\frac{\partial c}{\partial x} = 0, \quad u = \text{constant} > 0. \tag{3.1}$$

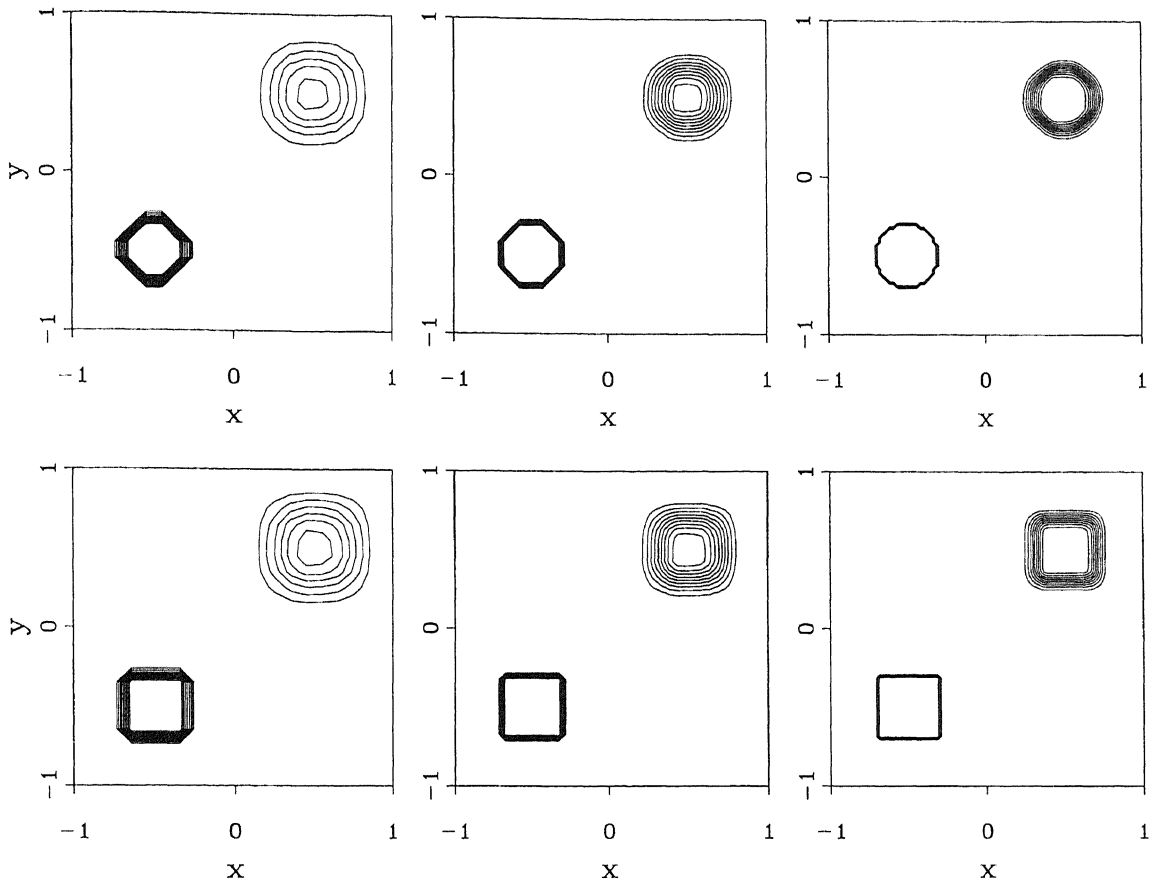

Fig. 3. Initial and final numerical solutions for convection circle (up) and square (down), through limited $k = \frac{1}{3}$-scheme, for from left to right: $h = \frac{1}{10}, \frac{1}{20}, \frac{1}{40}$.

Table 1
Numerical results for convection circle (up) and square (down), through limited $\kappa = \frac{1}{3}$-scheme

Circle	$h = \frac{1}{10}$	$h = \frac{1}{20}$	$h = \frac{1}{40}$
$\|\Delta c\|_1$	3.2×10^{-2}	1.7×10^{-2}	9.7×10^{-3}
$\|\Delta c\|_\infty$	5.7×10^{-1}	5.0×10^{-1}	5.1×10^{-1}
Square	$h = \frac{1}{10}$	$h = \frac{1}{20}$	$h = \frac{1}{40}$
$\|\Delta c\|_1$	3.6×10^{-2}	2.0×10^{-2}	1.2×10^{-2}
$\|\Delta c\|_\infty$	5.5×10^{-1}	6.2×10^{-1}	6.4×10^{-1}

Denoting the level-set function again by ψ, the extended equation reads

$$\frac{\partial q}{\partial t} + u\frac{\partial q}{\partial x} = 0, \quad q = \begin{pmatrix} c \\ \psi \end{pmatrix}, \quad u = \text{constant} > 0. \tag{3.2}$$

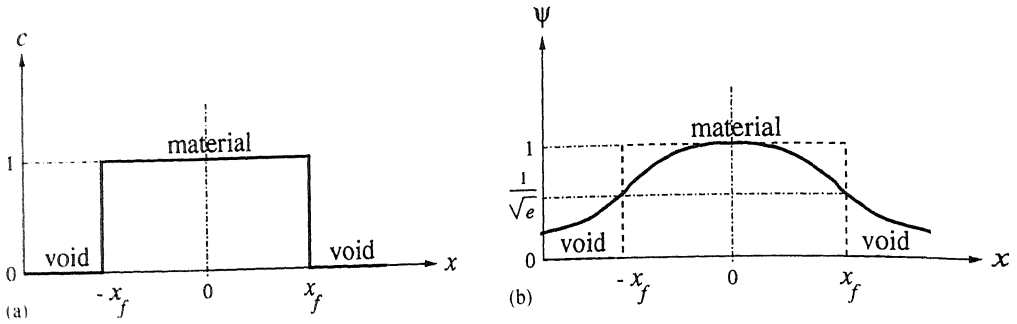

Fig. 4. Initial solutions. (a) Physical function; (b) level-set function.

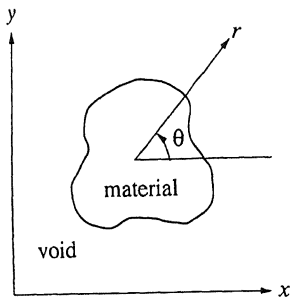

Fig. 5. 2-D material–void interface.

Suppose that the initial solution $c(x,t=0)$ looks as in the sketch in Fig. 4a, i.e., with the interfaces at $x=\pm x_f$ and with jumps from $c=1$ to $c=0$ over there. Then, for the corresponding initial distribution of the level-set function, $\psi(x,t=0)$, we propose the probability curve

$$\psi(x,t=0)=e^{-1.2(x/x_f)^2}. \tag{3.3}$$

A sketch of (3.3) is given in Fig. 4b. Note that (3.3) is infinitely many times differentiable at all points (including $x=0$, a linear level-set function would not be differentiable there). Higher-order accurate convection schemes can take full advantage of this differentiability. Further note that the function has been chosen such that its inflection points (its maximum slopes) coincide with the interfaces. (This gives the best posedness of the interface-detection problem.) In the level-set method, for the present 1-D model equation, a front is embedded in a 1-D function, while the front itself is a point-phenomenon only. This is typical for level-set methods: n-D physical fronts ($n=0$, 1 or 2) are embedded in $(n+1)$-D functions. We still remark that the choice (3.3) for the level-set function is rather arbitrary. Other functions, with equally good differentiation properties, and interface values ψ_f different from $1/\sqrt{e}$, could have been chosen.

For a multi-D problem, e.g., the 2-D problem of which the initial material–void interface is sketched in Fig. 5, the choice of the initial level-set function may be done in the following way. Take some point in the material and define that as the origin of a local r,θ-coordinate system (Fig. 5).

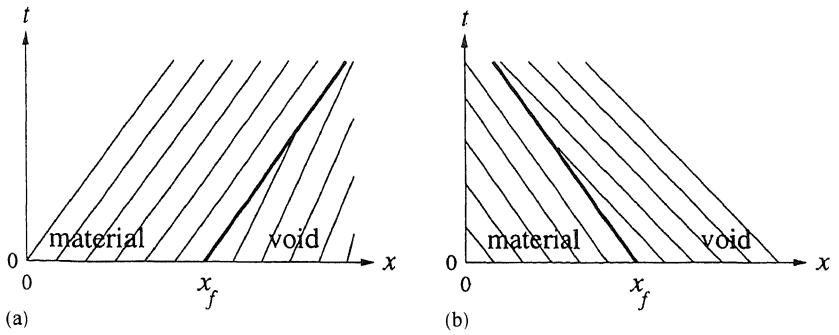

Fig. 6. Anti-convection for moving material–void interfaces. (a) Downstream-facing interface; (b) upstream-facing interface.

Next take as the initial level-set function

$$\psi(r,\theta,t=0)=\mathrm{e}^{-1/2(r/r_f)^2}, \tag{3.4}$$

where $r_f=r_f(\theta)$ is the radial distance from the point chosen to the material interface, for a given angle $\theta,\theta\in[0,2\pi]$. Doing so, we have $\psi_f=1/\sqrt{e}$ all over the interface. For many shapes, this initialization works, also in 3-D, where it carries over in a spherical coordinate system.

3.2. *Velocity field*

A subtle property of the convection of material–void interfaces is that the velocity field is only defined in the material. Hence, for the convection of the level-set function in the void region, an artificial velocity field still has to be defined. The opportunity to make this choice, without being inhibited by physics, is a good chance in fact to improve the free boundary's resolution. E.g., in the void region an artificial velocity can be chosen which counteracts the effects of numerical diffusion of the physical quantity c. For the 1-D convection equation (3.1), in the void region a velocity may be defined which looks as sketched in Fig. 6(a) and (b). So, for a downstream-facing front, $u\partial\psi/\partial x<0$, at the void side of the interface, a velocity may be chosen which is smaller than the velocity at the material side of the interface (Fig. 6(a)). This artificial anti-convection implies converging characteristics and may thus lead to re-steepening of a diffused front. To realize the steepening in case of an upstream-facing front, $u\partial\psi/\partial x>0$, the void velocity has to be taken greater than the material velocity (Fig. 6(b)).

Of course, difficulty here is to not affect too seriously the physically correct propagation speed of the front. Therefore, in this paper we do not apply anti-convection. (In [1], the idea of anti-convection *has* been applied.) Our present suggestion for the choice of the artificial velocity field in the void region is to take that as the smoothest possible extrapolation of the velocity field at the material interface. In case of a constant velocity at the interface, one defines that specific velocity as the velocity in the entire void region. In case of a non-constant velocity at the interface, we suggest to take that velocity distribution, say $q_{\mathrm{in}}=q_{\mathrm{in}}(\theta)$ (Fig. 7) as the inner boundary condition for an elliptic (Laplacian) boundary-value problem, defined for the artificial velocity in the void region. As the boundary condition at the outer boundary of the void region, q_{out} (Fig. 7),

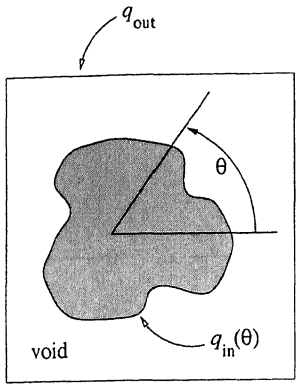

Fig. 7. Void region.

one can take the average velocity at the material interface. So, in 2-D, this elliptic velocity gener amounts to solving

$$\Delta q = 0, \quad q = \begin{pmatrix} u \\ v \end{pmatrix}, \quad q_{in} = q_{in}(\theta), \quad q_{out} = \frac{1}{2\pi} \int_0^{2\pi} q_{in}(\theta)\, d\theta. \tag{(}$$

3.3. Simple level-set results: shape tracking only

For the two test cases defined in Section 2.1, we can already present practically relevant leve results now, viz. for the convection of the geometry. As the local origins of the r,θ-coordi system introduced in Section 3.1, we simply take the centers of gravity of the initial circle and initial square. For the initial function $\psi(r,\theta,t=0)$ we take (3.4) and for its numerical convec scheme the non-limited $\kappa = \frac{1}{3}$-scheme. So, as mentioned, the level-set function is simply embe into the existing discretization, with as the only difference that for the level-set function the limit switched off. Thus, for completeness, at the vertical cell faces $\partial\Omega_{i+1/2,j}$, $i = 0, 1, \ldots, n$, $j = 1, 2,$. we take

$$\psi_{i+\frac{1}{2},j} = \begin{cases} i=0: & (\psi_{\text{exact}})_{1/2,j} = e^{-1/2(r_{1/2,j}(t)/r_f(t))^2}, \\ i=1: & \frac{1}{2}(\psi_{1,j} + \psi_{2,j}), \\ i=n: & \psi_{n,j} + \frac{1}{2}(\psi_{n,j} - \psi_{n-1,j}), \\ \text{else:} & \psi_{i,j} + \frac{1+\kappa}{4}(\psi_{i+1,j} - \psi_{i,j}) + \frac{1-\kappa}{4}(\psi_{i,j} - \psi_{i-1,j}), \quad \kappa = \frac{1}{3}, \end{cases} \tag{3}$$

and likewise, at the horizontal cell faces $\partial\Omega_{i,j+1/2}$, $i = 1, 2, \ldots, n$, $j = 0, 1, \ldots, n$

$$\psi_{i,j+\frac{1}{2}} = \begin{cases} j=0: & (\psi_{\text{exact}})_{i,1/2} = e^{-1/2(r_{i,1/2}(t)/r_f(t))^2}, \\ j=1: & \frac{1}{2}(\psi_{i,1} + \psi_{i,2}), \\ j=n: & \psi_{i,n} + \frac{1}{2}(\psi_{i,n} - \psi_{i,n-1}), \\ \text{else:} & \psi_{i,j} + \frac{1+\kappa}{4}(\psi_{i,j+1} - \psi_{i,j}) + \frac{1-\kappa}{4}(\psi_{i,j} - \psi_{i,j-1}), \quad \kappa = \frac{1}{3}, \end{cases} \tag{3}$$

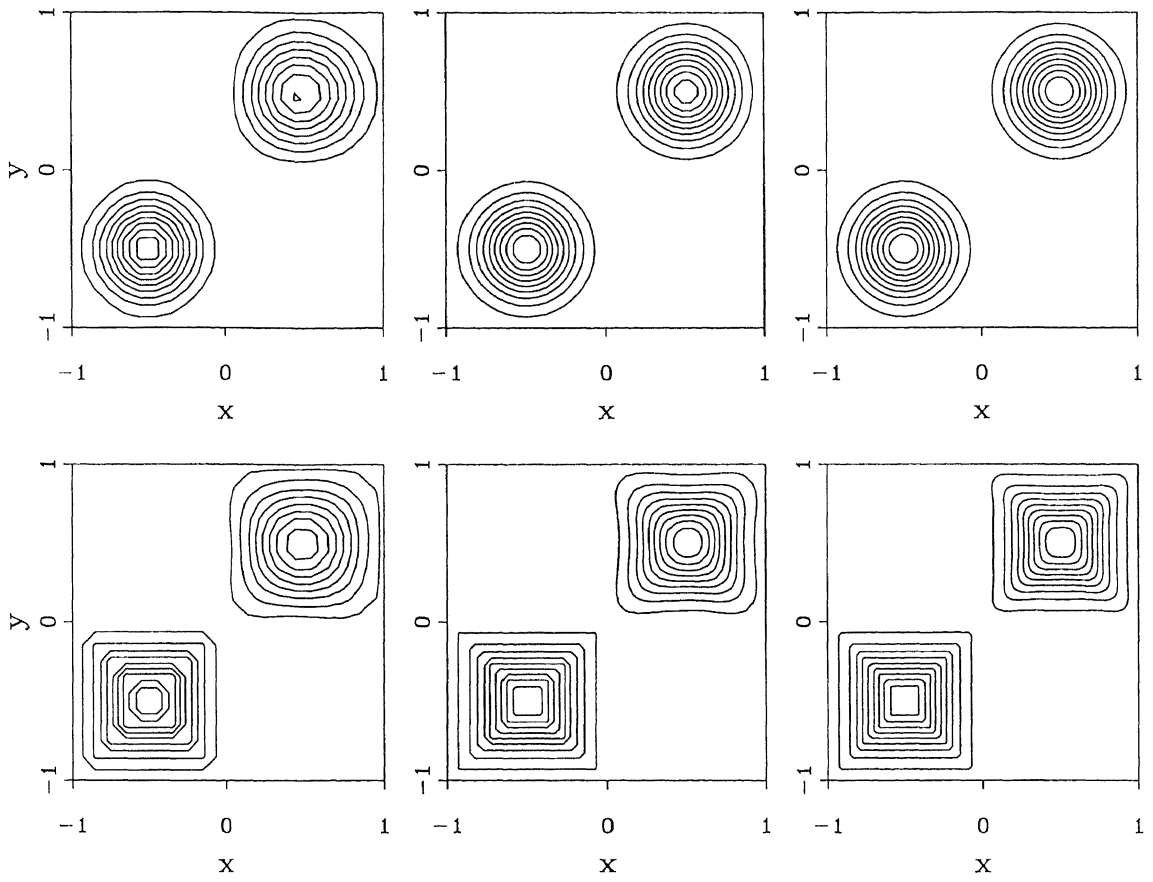

Fig. 8. Initial and final numerical solutions for convection circular (up) and square (down) level-set function ψ, through non-limited $\kappa = \frac{1}{3}$-scheme, for from left to right: $h = \frac{1}{10}, \frac{1}{20}, \frac{1}{40}$.

with the radii $r_{1/2,j}(t), r_{i,1/2}(t)$ and $r_f(t)$ exact for both the circular and the square shape. Applying the identical time integration as in Section 2.2, the results depicted in Fig. 8 are obtained.

As in Tables 1 and 2, we give some more quantitative information about the numerical level-set solutions. As expected, higher-order accuracy *is* obtained here. For the circular shape, $\|\Delta\psi\|_1$ behaves almost third-order accurate. For the square solution, due to the nonsmoothness at the four corners, the accuracy behavior is less good: second-order almost, which is still better nevertheless than the orders of accuracy to be observed in Table 1.

Now the possibility also exists to compare the shape preservation properties of both approaches: the standard numerical (limited $\kappa = \frac{1}{3}$) approach from Section 2.2 and the present level-set approach. For additional comparison purposes, we also consider the corresponding, exact discrete solutions. For both the exact discrete solution and the solution obtained by the standard approach, the material interface is defined as the iso-line $c_f \equiv h$ (h being the mesh width). In the standard approach, as mentioned in Section 1.3, just a proper definition of the material interface is not trivial already. In the

Table 2
Numerical results for convection circular (up) and square (down) level-set function, through nonlimited $\kappa = \frac{1}{3}$-scheme

Circular	$h = \frac{1}{10}$	$h = \frac{1}{20}$	$h = \frac{1}{40}$
$\|\Delta\psi\|_1$	9.5×10^{-3}	1.5×10^{-3}	1.9×10^{-4}
$\|\Delta\psi\|_\infty$	1.6×10^{-1}	3.4×10^{-2}	4.8×10^{-3}
Square	$h = \frac{1}{10}$	$h = \frac{1}{20}$	$h = \frac{1}{40}$
$\|\Delta\psi\|_1$	1.4×10^{-2}	4.4×10^{-3}	1.4×10^{-3}
$\|\Delta\psi\|_\infty$	1.5×10^{-1}	9.3×10^{-2}	5.0×10^{-2}

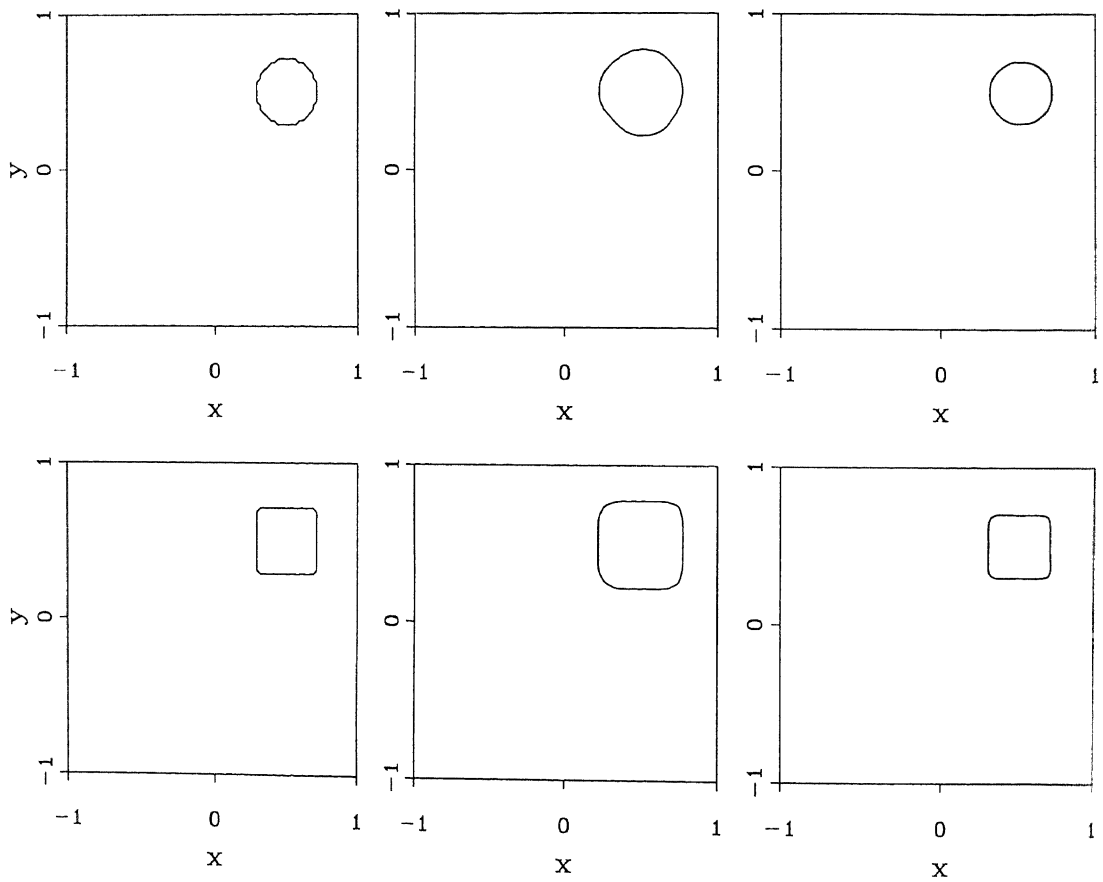

Fig. 9. Final shapes for circle (up) and square (down), for $h = \frac{1}{40}$ and according to, from left to right: exact discrete solution c (iso-line $c = c_f = h$), limited $\kappa = \frac{1}{3}$-solution c (iso-line $c = c_f = h$) and nonlimited $\kappa = \frac{1}{3}$-solution ψ (iso-line $\psi = \psi_f = \frac{1}{\sqrt{e}}$).

level-set approach, this definition already exists: the iso-line $\psi_f \equiv 1/\sqrt{e}$. For the 80×80-grid, in Fig. 9, we present discrete shapes at $t=1$, from left to right: (i) according to the exact discrete solution c, (ii) according to the limited $\kappa=\frac{1}{3}$ solution c and (iii) according to the nonlimited $\kappa=\frac{1}{3}$ solution ψ. (The iso-lines in the two most left graphs of Fig. 9 belong to the same solutions that have already been depicted in the two most right graphs of Fig. 1, and (likewise) the two middle graphs in Fig. 9 belong to the same solutions already depicted in the two most right graphs in Fig. 3.) For the circle, the difference in quality between the standard numerical results and the level-set results is striking. Seen from Fig. 9, the shape preservation of the level-set circle is very good; numerical errors are very small. The depicted level-set circle is even more accurate than the plotted, exact discrete circle. The quality of the latter suffers from the interface-definition problem. For the square, the level-set solution is less accurate than for the circle (because of the loss of one order of accuracy at the corners). Nevertheless, here as well, the level-set result is still much better than the standard numerical result in the middle graph.

4. Extended level-set results: Feedback with physics

The level-set results presented in the previous section are worthwhile. However, in practical applications, shape preservation may not be the only goal. An accurate resolution of physical quantities at the interface may also be of interest. E.g., in a real fluid dynamics problem, the velocity components at the interface are a particularly important issue, since they determine the motion of the free surface. Also, the density distribution along and near the interface may be of interest. Note that, so far, we do have obtained good shape preservation (the two right graphs in Fig. 9), but a physical quantity as density will still be diffused at the interface (as demonstrated in the two middle graphs of Fig. 9). However, with the level-set function and equation added to a system of physical conservation laws, the useful knowledge to be extracted from the numerical solution of the level-set function does not need to be restricted to geometrical improvement of the free boundary only. Knowledge obtained from the level-set solution can also be fed back into the discretization of the physical equations. This feedback of the level-set function to physics is application-dependent and much effort may be put into it. Already for the present model for moving material–void interfaces, despite the model's simplicity, it has appeared that defining the feedback is not straightforward; many possibilities exist. In [12], various feedback schemes are presented. Here, we present two such schemes. The model equation to be considered still is

$$\frac{\partial q}{\partial t}+u\frac{\partial q}{\partial x}+v\frac{\partial q}{\partial y}=0, \quad q=\begin{pmatrix} c \\ \psi \end{pmatrix}, \quad u=v=1. \tag{4.1}$$

4.1. First feedback

The decoupled discretization of system (4.1) is given by (2.6), (2.7) and (3.6). in making the physical coupling, we maintain discretization (3.6) for the level-set function, but we extend (2.6). A seemingly obvious physical argument for making this extension for the present (model) interfaces is that in the void region, the physical fluxes must be zero. In here, a subtle case is the multi-D situation as sketched in Fig. 10, i.e., a situation in which the iso-line $\psi=\psi_f$ (the material interface)

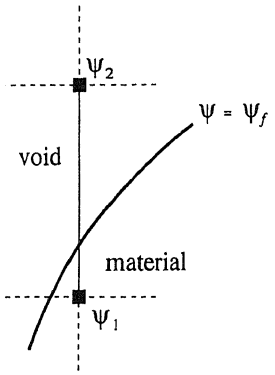

Fig. 10. Material–void interface cutting cell face.

cuts the cell face considered and where the corresponding cell-face value — say $\psi_{i+1/2,j}$ — is less than ψ_f. In such a case, the cell face should be left open. To realize this, we propose the following scheme. First, we approximate the cell-vertex values ψ_1 and ψ_2 (Fig. 10). For the vertical cell faces $\partial\Omega_{i+1/2,j}$, $i = 0,1,\ldots,n$, $j = 1,2,\ldots,n$, these node values can be approximated by

$$(\psi_1)_{i+1/2,j} = \begin{cases} j = 1: & \psi_{i+1/2,1} + \frac{1}{2}(\psi_{i+1/2,1} - \psi_{i+1/2,2}), \\ \text{else:} & \frac{1}{2}(\psi_{i+1/2,j-1} + \psi_{i+1/2,j}), \end{cases} \tag{4.2a}$$

$$(\psi_2)_{i+1/2,j} = \begin{cases} j = n: & \psi_{i+1/2,n} + \frac{1}{2}(\psi_{i+1/2,n} - \psi_{i+1/2,n-1}), \\ \text{else:} & \frac{1}{2}(\psi_{i+1/2,j} + \psi_{i+1/2,j+1}), \end{cases} \tag{4.2b}$$

with $\psi_{i+1/2,j}$ according to (3.6a). For the horizontal cell faces $\partial\Omega_{i,j+1/2}$, $i = 1,2,\ldots,n$, $j = 0,1,\ldots,n$ we have

$$(\psi_1)_{i,j+1/2} = \begin{cases} i = 1: & \psi_{1,j+1/2} + \frac{1}{2}(\psi_{1,j+1/2} - \psi_{2,j+1/2}), \\ \text{else:} & \frac{1}{2}(\psi_{i-1,j+1/2} + \psi_{i,j+1/2}), \end{cases} \tag{4.3a}$$

$$(\psi_2)_{i,j+1/2} = \begin{cases} i = n: & \psi_{n,j+1/2} + \frac{1}{2}(\psi_{n,j+1/2} - \psi_{n-1,j+1/2}), \\ \text{else:} & \frac{1}{2}(\psi_{i,j+1/2} + \psi_{i+1,j+1/2}), \end{cases} \tag{4.3b}$$

with $\psi_{i,j+1/2}$ according to (3.6b). Then, at the vertical cell face $\partial\Omega_{i+1/2,j}$, the first feedback scheme is

$$c_{i+1/2,j} = \begin{cases} ((\psi_1)_{i+1/2,j} - \psi_f)((\psi_2)_{i+1/2,j} - \psi_f) < 0: & \text{according to (2.6a) and (2.7),} \\ \text{else:} & \max\left(0, \frac{\psi_{i+1/2,j} - \psi_f}{|\psi_{i+1/2,j} - \psi_f|}\right) c_{i+1/2,j}, \end{cases} \tag{4.4a}$$

and at the horizontal cell face $\partial\Omega_{i,j+1/2}$

$$c_{i,j+1/2} = \begin{cases} ((\psi_1)_{i,j+1/2} - \psi_f)((\psi_2)_{i,j+1/2} - \psi_f) < 0: & \text{according to (2.6b) and (2.7),} \\ \text{else:} & \max\left(0, \frac{\psi_{i,j+1/2} - \psi_f}{|\psi_{i,j+1/2} - \psi_f|}\right) c_{i,j+1/2}, \end{cases} \tag{4.4b}$$

where $c_{i+1/2,j}$ and $c_{i,j+1/2}$ in the right-hand sides are determined by (2.6) with limiter (2.7), and $\psi_{i+1/2,j}$ and $\psi_{i,j+1/2}$ again by (3.6).

So, note that in (4.4), in fact, an extra limiting may be applied to the physical fluxes, a limiting controlled by the level-set function. The level-set limiting is binary; it either opens or closes cell faces. In the void region ($\psi < \psi_f$) it may close cell faces. This obviously inhibits numerical diffusion into the void region. Note that to still preserve monotonicity, the original limiter $\phi(r)$ is still necessary. Since the binary limiter can have the values zero and one only, it cannot affect this monotonicity. Finally, note that the level-set limiter, with its ability to close cell faces, does not affect conservation; the basic finite-volume scheme remains unchanged. (What flows out of or into a cell across a face, remains to flow into or out of the cell neighboring that face.)

Numerical results obtained with this fed back scheme for each of the two test cases, are given in [12]. The results are not yet good; in the upstream void region, small amounts of mass may stagnate, they are pent up in cells with faces closed by the level-set limiter. The cause is clear; if in a cell $\Omega_{i,j}, \psi_{i-1/2,j}, \psi_{i+1/2,j}, \psi_{i,j-1/2}$ as well as $\psi_{i,j+1/2}$ are less than ψ_f and if the iso-line $\psi = \psi_f$ does not cut any of the four cell faces $\partial\Omega_{i-1/2,j}, \partial\Omega_{i+1/2,j}, \partial\Omega_{i,j-1/2}$ and $\partial\Omega_{i,j+1/2}$, then all these four faces are closed, irrespective of the fact that there is still some mass in that cell ($c_{i,j} > 0$).

4.2. Improved feedback

In improving the feedback, closure of cell faces will be done at the downstream sides of fronts only. In the upstream void region, an appropriate limiter will be applied: the superbee limiter [16]:

$$\phi(r) = \begin{cases} 0, & r \leqslant 0, \\ 2r, & 0 < r \leqslant \frac{1}{2}, \\ 1, & \frac{1}{2} < r \leqslant 1, \\ r, & 1 < r \leqslant 2, \\ 2 & \text{else.} \end{cases} \tag{4.5}$$

Because it is compressive, the superbee limiter will counteract diffusion of the interface. Besides a front itself, its downstream and upstream sides can also be accurately distinguished by means of the level-set function. In 2-D, the downstream region is there where

$$(u, v) \cdot \nabla\psi < 0. \tag{4.6}$$

The required cell-face gradient $\nabla\psi$ can be evaluated in more or less the standard second-order accurate way, as described in, e.g., Section 3.7 in [14]. For the present simple test problems (with all horizontal cell faces aligned to the x-axis and all vertical cell faces aligned to the y-axis, and with the grid equidistant and $h_x = h_y = h$), this gradient evaluation becomes, at the vertical cell faces

$\partial\Omega_{i+\frac{1}{2},j}$, $i=0,1,\ldots,n$, $j=1,2,\ldots,n$:

$$(\nabla\psi)_{i+1/2,j}=\begin{pmatrix}\left(\dfrac{\partial\psi}{\partial x}\right)_{i+1/2,j}=\begin{cases}i=0: & \frac{1}{3h}(-8\psi_{1/2,j}+9\psi_{1,j}-\psi_{2,j})\\ i=n: & \frac{1}{3h}(8\psi_{n+1/2,j}-9\psi_{n,j}+\psi_{n-1,j})\\ \text{else:} & \frac{1}{h}(\psi_{i+1,j}-\psi_{i,j})\end{cases}\\[2ex]\left(\dfrac{\partial\psi}{\partial y}\right)_{i+1/2,j}=\begin{cases}j=1: & \frac{1}{2h}(-3\psi_{i+1/2,1}+4\psi_{i+1/2,2}-\psi_{i+1/2,3})\\ j=n: & \frac{1}{2h}(3\psi_{i+1/2,n}-4\psi_{i+1/2,n-1}+\psi_{i+1/2,n-2})\\ \text{else:} & \frac{1}{2h}(\psi_{i+1/2,j+1}-\psi_{i+1/2,j-1})\end{cases}\end{pmatrix}, \tag{4.7a}$$

and at the horizontal cell faces $\partial\Omega_{i,j+1/2}$, $i=1,2,\ldots,n$, $j=0,1,\ldots,n$:

$$(\nabla\psi)_{i,j+1/2}=\begin{pmatrix}\left(\dfrac{\partial\psi}{\partial x}\right)_{i,j+1/2}=\begin{cases}i=1: & \frac{1}{2h}(-3\psi_{1,j+1/2}+4\psi_{2,j+1/2}-\psi_{3,j+1/2})\\ i=n: & \frac{1}{2h}(3\psi_{n,j+1/2}-4\psi_{n-1,j+1/2}+\psi_{n-2,j+1/2})\\ \text{else:} & \frac{1}{2h}(\psi_{i+1,j+1/2}-\psi_{i-1,j+1/2})\end{cases}\\[2ex]\left(\dfrac{\partial\psi}{\partial y}\right)_{i,j+1/2}=\begin{cases}j=0: & \frac{1}{3h}(-8\psi_{i,1/2}+9\psi_{i,1}-\psi_{i,2})\\ j=n: & \frac{1}{3h}(8\psi_{i,n+1/2}-9\psi_{i,n}+\psi_{i,n-1})\\ \text{else:} & \frac{1}{h}(\psi_{i,j+1}-\psi_{i,j})\end{cases}\end{pmatrix}. \tag{4.7b}$$

Now the complete flux formulae can be given. At the vertical cell faces we take:

$\psi_{i+1/2,j}$ according to (3.6a),

$$\psi_{i+1/2,j}<\psi_f:\begin{cases}\nabla\psi_{i+1/2,j}\text{ according to (4.7a),}\\ (u,v)\cdot\nabla\psi_{i+1/2,j}<0: & c_{i+1/2,j}\text{ according to (4.2) and (4.4a),}\\ \text{else:} & c_{i+1/2,j}\text{ according to (2.6a) and (4.5),}\end{cases}$$

$$\text{else:}\qquad c_{i+1/2,j}\text{ according to (2.6a) and (2.7).} \tag{4.8a}$$

And, similarly, at the horizontal cell faces:

$\psi_{i,j+1/2}$ according to (3.6b),

$$\psi_{i,j+1/2}<\psi_f:\begin{cases}\nabla\psi_{i,j+1/2}\text{ according to (4.7b),}\\ (u,v)\cdot\nabla\psi_{i,j+1/2}<0: & c_{i,j+1/2}\text{ according to (4.3) and (4.4b),}\\ \text{else:} & c_{i,j+1/2}\text{ according to (2.6b) and (4.5),}\end{cases}$$

$$\text{else:}\qquad c_{i,j+1/2}\text{ according to (2.6b) and (2.7).} \tag{4.8b}$$

In Fig. 11, numerical results are presented for this approach. In the Tables 3(a) and (b), we give some quantitative information about the numerical solutions. In comparison with the results given in Table 1, an improvement of $\|\Delta c\|_1$ has been obtained. A flaw in the solutions obtained for the convected square still is the crosswise diffusion at the diagonally opposite corner points where the discretization changes type. A fix to this will probably be to make the transition between both schemes smoother.

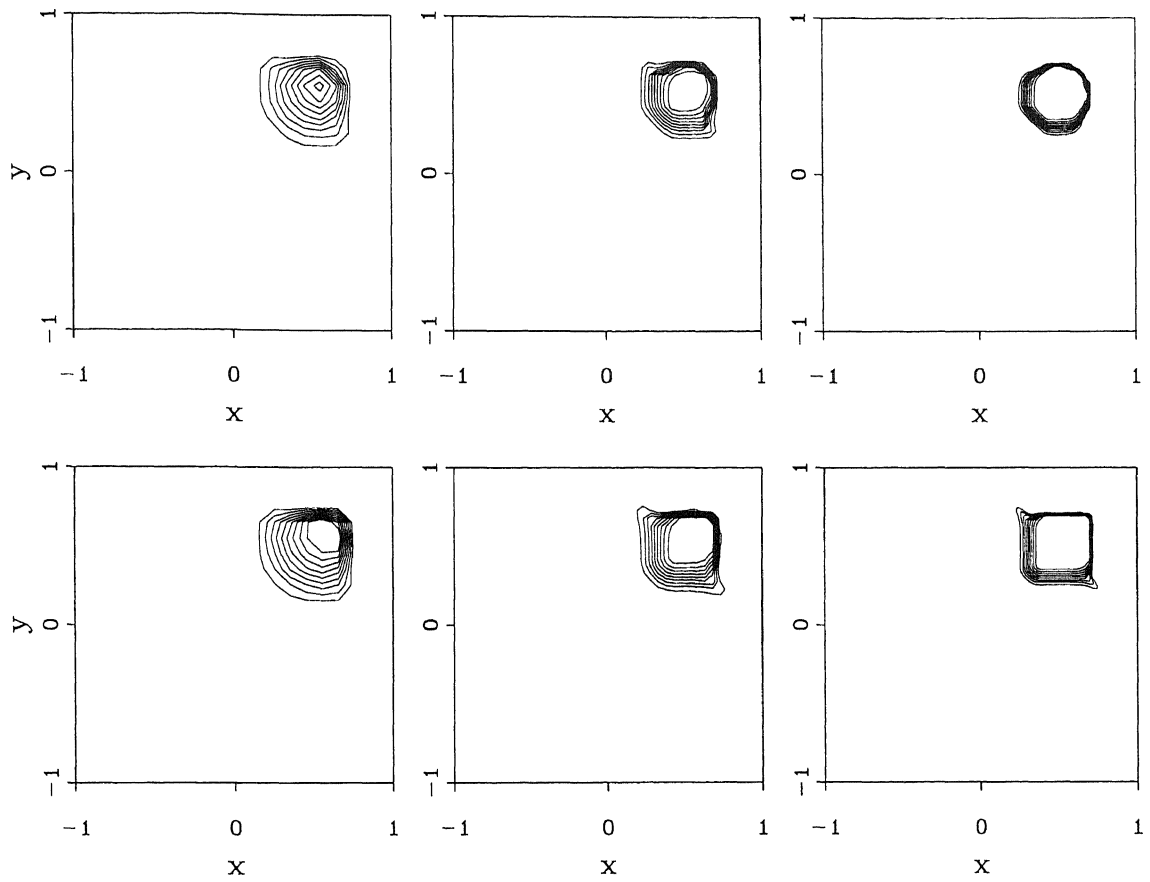

Fig. 11. Numerical solutions c for convection circle (up) and square (down), through fed back level-set scheme, for from left to right: $h = \frac{1}{10}, \frac{1}{20}, \frac{1}{40}$.

Table 3
Numerical results for convection circle and square, through fed back level-set scheme

Circle	$h = \frac{1}{10}$	$h = \frac{1}{20}$	$h = \frac{1}{40}$
$\|\Delta c\|_1$	2.0×10^{-2}	1.1×10^{-2}	5.4×10^{-3}
$\|\Delta c\|_\infty$	5.4×10^{-1}	5.7×10^{-1}	5.5×10^{-1}
Square	$h = \frac{1}{10}$	$h = \frac{1}{20}$	$h = \frac{1}{40}$
$\|\Delta c\|_1$	2.0×10^{-2}	1.3×10^{-2}	7.2×10^{-3}
$\|\Delta c\|_\infty$	5.9×10^{-1}	6.0×10^{-1}	6.7×10^{-1}

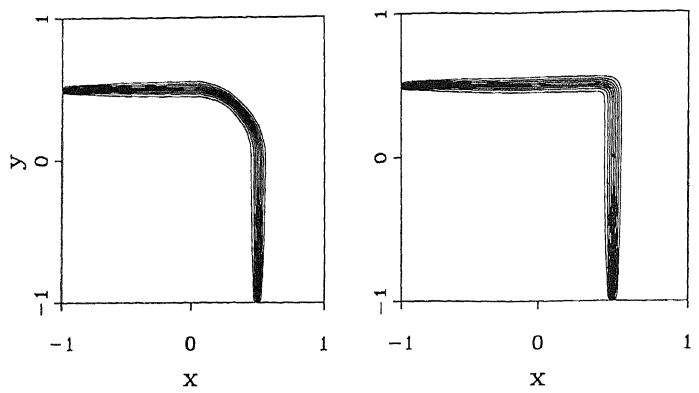

Fig. 12. Curvilinear (left) and rectilinear (right) numerical solutions c for convection downstream-facing interfaces, through standard (limited $\kappa = \frac{1}{3}$) scheme ($h = \frac{1}{40}$).

In Section 4.1 of [5], Cocchi and Saurel present results for a test case comparable to the present diagonal convection of a square. (Cocchi and Saurel consider the diagonal convection of a square gas bubble.) In Fig. 24 of their paper, they show that they can accurately resolve a physical quantity (the density), not only at the downstream-facing part but also at the upstream-facing part of the interface. This difference with our results can be explained from the difference in methods; Cocchi and Saurel apply a sophisticated front-tracking method (with markers attached to the interface), whereas we apply a plain capturing method, without subcell resolution.

From the results in Fig. 11, it appears that the solution quality is particularly good at the downstream-facing interfaces. We illustrate this once more by means of the following simplifications of the two model problems. The equation and velocity to be considered are still the same, i.e., (2.1) and (2.3), respectively, but the initial solutions differ. Instead of (2.2a), first we consider a downstream-facing curvilinear front only, viz.

$$c(x,y,t=0)=\begin{cases}1, & (x,y)\in(x-x_c)^2+(y-y_c)^2\leqslant(\frac{1}{2})^2, \quad x_c=y_c=-1,\\ 0 & \text{elsewhere,}\end{cases} \tag{4.9a}$$

and likewise, instead of (2.2b), the downstream-facing rectilinear front

$$c(x,y,t=0)=\begin{cases}1, & (x,y)\in[x_c,y_c]\times[x_c+\frac{1}{2},y_c+\frac{1}{2}], \quad x_c=y_c=-1,\\ 0 & \text{elsewhere.}\end{cases} \tag{4.9b}$$

For both fronts, the corresponding boundary conditions are

$$c(x=-1,y,t)=\begin{cases}1, & y\leqslant(y_c+\frac{1}{2})+vt,\\ 0 & \text{elsewhere,}\end{cases} \tag{4.10a}$$

$$c(x,y=-1,t)=\begin{cases}1, & x\leqslant(x_c+\frac{1}{2})+ut,\\ 0 & \text{elsewhere.}\end{cases} \tag{4.10b}$$

In Fig. 12, the numerical solutions c at $t=1$ are given, as obtained with the standard (i.e., the limited $\kappa=\frac{1}{3}$) scheme. In Fig. 13, the corresponding results obtained with the fed back level-set

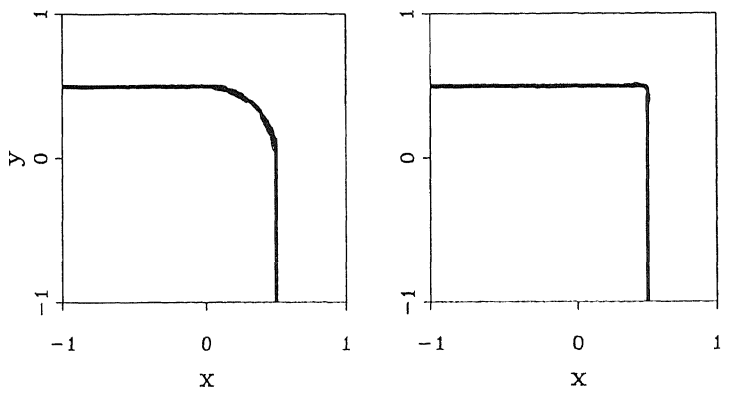

Fig. 13. Curvilinear (left) and rectilinear (right) numerical solutions c for convection downstream-facing interfaces, through fed back level-set scheme ($h = \frac{1}{40}$).

approach are shown. Observation learns that the effect of closure of cell faces in the void region does not only lead to a thinning of the interface part diffused into the void region, but also to a thinning of the part diffused into the material.

5. Conclusions

For capturing free boundaries in an Eulerian formulation, the known advantages of level-set methods over most alternative Eulerian techniques are:

- level-set methods are smooth at physical discontinuities and, hence, allow us to maintain maximum numerical accuracy there,
- through the level-set function, the location of the discontinuity is clearly defined,
- the level-set function can be simply embedded in the system of physical equations and can be discretized collectively and consistently with these,
- there is no principal difficulty in extending a level-set method from 2-D to 3-D.

An additional advantage presented and worked out in this paper is that:

- the possibility exists to convect the level-set function as an active (instead of as a passive) scalar, i.e., to directly feed it back into the discretization of the physical equations (into the flux computations).

Based on the model studies presented in this paper, the following foreknowledge exists about the development of a level-set method for material–void interface problems. For shape-tracking purposes only, as expected, the level-set approach without feedback yields excellent results. When feeding information about the level-set function back into the discretization of the physical equations, for downstream-facing material–void interfaces strongly improved physical results can be obtained as well. For upstream-facing fronts, so far, the gains obtained through feedback are less good. Here, the fed back level-set method is still open for further improvement. For problems with both downstream- and upstream-facing fronts, the challenge is to properly combine three different discretizations: that in the upstream void region, that in the downstream void region and that in the material domain. Given the foregoing list of advantages, further research is worth the effort.

Acknowledgement

We thank the referees for their suggestions to improve this paper.

References

[1] C. Aalburg, Experiments in minimizing numerical diffusion across a material boundary, M.Sc. Thesis, Department of Aerospace Engineering, University of Michigan, Ann Arbor, 1996. Also: http://www.engin.umich.edu/research/cfd/publications/publications.html.
[2] Y.C. Chang, T.Y. Hou, B. Merriman, S. Osher, A level set formulation of Eulerian interface capturing methods for incompressible fluid flows, J. Comput. Phys. 124 (1996) 449–464.
[3] S. Chen, B. Merriman, S. Osher, P. Smereka, A simple level-set method for solving Stefan problems, J. Comput. Phys. 135 (1997) 8–29.
[4] A.J. Chorin, Flame advection and propagation algorithms, J. Comput. Phys. 35 (1980) 1–11.
[5] J.-P. Cocchi, R. Saurel, A Riemann problem based method for the resolution of compressible multimaterial flows, J. Comput. Phys. 137 (1997) 265–298.
[6] S.F. Davis, An interface tracking method for hyperbolic systems of conservation laws, Appl. Numer. Math. 10 (1992) 447–472.
[7] F.H. Harlow, J.E. Welch, Numerical calculation of time-dependent viscous incompressible flow of fluid with free surfaces, Phys. Fluids 8 (1965) 2182–2189.
[8] C.W. Hirt, B.D. Nicholls, Volume of fluid (VOF) method for dynamics of free boundaries, J. Comput. Phys. 39 (1981) 201–225.
[9] T.Y. Hou, Z. Li, S. Osher, H. Zhao, A hybrid method for moving interface problems with application to the Hele-Shaw flow, J. Comput. Phys. 134 (1997) 236–252.
[10] W. Hundsdorfer, B. Koren, M. van Loon, J.G. Verwer, A positive finite-difference advection scheme, J. Comput. Phys. 117 (1995) 35–46.
[11] B. Koren, A robust upwind discretization method for advection, diffusion and source terms, in: C.B. Vreugdenhil, B. Koren (Eds.), Numerical Methods for Advection–Diffusion Problems, Notes on Numerical Fluid Mechanics, vol. 45, Vieweg, Braunschweig, 1993, pp. 117–138.
[12] B. Koren, A.C.J. Venis, A level-set method for moving material–void interfaces, Report MAS-R9731, CWI, Amsterdam, 1997. Also: http://www.cwi.nl/static/publications/reports/MAS-1997.html.
[13] W. Mulder, S. Osher, J.A. Sethian, Computing interface motion in compressible gas dynamics, J. Comput. Phys. 100 (1992) 209–228.
[14] R. Peyret, T.D. Taylor, Computational Methods for Fluid Flow, Springer, Berlin, 1983.
[15] S. Osher, J.A. Sethian, Fronts propagating with curvature-dependent speed: algorithms based on Hamilton–Jacobi formulations, J. Comput. Phys. 79 (1988) 12–49.
[16] P.L. Roe, Some contributions to the modelling of discontinuous flows, in: B.E. Engquist, S. Osher, R.C.J. Somerville (Eds.), Large-Scale Computations in Fluid Mechanics, Lectures in Applied Mathematics 22, Part 2, American Mathematical Society, Providence, RI, 1985, pp. 163–193.
[17] J.A. Sethian, Level-Set Methods: Evolving Interfaces in Geometry, Fluid Mechanics, Computer Vision, and Materials Science, Cambridge University Press, Cambridge, 1996.
[18] M. Sussman, P. Smereka, S. Osher, A level set approach for computing solutions to incompressible two-phase flow, J. Comput. Phys. 114 (1994) 146–159.
[19] P.K. Sweby, High resolution schemes using flux limiters for hyperbolic conservation laws, SIAM J. Numer. Anal. 21 (1984) 995–1011.
[20] H.-K. Zhao, T. Chan, B. Merriman, S. Osher, A variational level set approach to multiphase motion, J. Comput. Phys. 127 (1996) 179–195.